

Copyright © [2008] IEEE. Reprinted from IEEE International Geoscience & Remote Sensing, Vol. 2, July 2008.

This material is posted here with permission of the IEEE. Internal or personal use of this material is permitted. However, permission to reprint/republish this material for advertising or promotional purposes or for creating new collective works for resale or redistribution must be obtained from the IEEE by writing to [pubs-permissions@ieee.org](mailto:pubs-permissions@ieee.org). By choosing to view this document, you agree to all provisions of the copyright laws protecting it.

# HYPERSPECTRAL DETECTION AND IDENTIFICATION WITH CONSTRAINED TARGET SUBSPACES

*S. Adler-Golden, J. Gruninger and R. Sundberg*

Spectral Sciences, Inc., Burlington MA 01803-3304

## ABSTRACT

Subspace methods for hyperspectral imagery enable detection and identification of targets under unknown environmental conditions by specifying a subspace of possible target spectral signatures (and, optionally, a background subspace) and identifying closely fitting spectra in the image. In this study, detection performance in the thermal infrared (IR) was compared using various constrained and unconstrained basis set expansions of low-dimensional target subspaces. An initial investigation of detection using retrieved atmospheric parameters to reduce subspace size and/or dimensionality has also been performed.

**Index Terms**— hyperspectral, subspace, invariant, detection, infrared

## 1. INTRODUCTION

Hyperspectral imaging (HSI) from airborne or space-based platforms is a valuable technology for detecting and classifying materials and objects on the Earth's surface based on their spectral signatures. Analysis of these data is challenging, however, as the signatures contain variable atmospheric components and surface spectral properties. In the solar wavelength region there are well-established atmospheric correction or "compensation" methods for removing atmospheric effects and retrieving surface reflectance [1]. For thermal IR HSI sensors, analogous methods exist for retrieving surface emissivity [2-4], but they tend to be more complex, less accurate, and more computationally intensive due to the need to retrieve temperature information.

An alternative analysis approach that is especially attractive in the thermal IR is based on radiance spectrum simulation. First-principles simulations are used to develop a comprehensive dataset of potential target spectral signatures, encompassing a broad range of atmospheric conditions, surface temperature, etc. For whole-pixel detection, the results are compared to the measured pixel spectra; a good match (low residual) suggests that the pixel contains the target in question; a poor match indicates otherwise. This approach becomes practical with an efficient matching algorithm. In the "invariant" subspace approach of Healey and Slater [5], the target dataset, which includes all possible sources of variability, is compressed down to a small subspace of singular value decomposition (SVD) basis vectors. To find a whole-pixel target, the pixel spectra  $L$  are fit using this basis set, and an error residual is computed and thresholded. Healey and Slater fit amplitude-normalized pixel spectra and calculate the root-sum-square (RSS) error residual; this is equivalent to normalizing RSS error to the pixel spectrum amplitude, i.e.,

$$\sigma_n = \|L - \sum \alpha_j m_j\| / \|L\| \quad (1a)$$

Here the  $m_j$  are the SVD basis vectors,  $\alpha_j$  are the coefficients of the fit, and the double bars denote Euclidean norm. The invariant approach was later extended to the detection of subpixel targets [6] by modeling the subpixel background as a second subspace, using background basis vectors as additional fitting components. Later work on subpixel detection has employed different types of basis sets, including an endmember basis set [7]. We note that a slightly more efficient basis set can be generated by subtracting the mean of the subspace spectra prior to performing the SVD. Here fitting error is not proportional to amplitude, so a non-normalized error expression

$$\sigma'_n = \|L' - \sum \alpha'_j m'_j\| \quad (1b)$$

is appropriate, where the  $m'_j$  are the SVD basis vectors of the mean-subtracted target subspace,  $L'$  is the pixel spectrum after subtraction of the target mean, and the  $\alpha'_j$  are the coefficients of the fit to  $L'$ .

The subspace approach is very flexible, allowing it to be tailored to a variety of remote sensing problems. For example, when atmospheric parameters are known from weather data but range to the target and surface temperature are unknown, there are only two dimensions in the target subspace, which can be represented with far fewer SVD basis vectors than the typical ten or so used by Healey *et al.* [5,6]. This reduction in dimensionality improves detection performance. The subspace approach is also amenable to detecting objects with intrinsic variability.

A limitation of existing subspace methods is that the size (as distinguished from dimensionality) of the subspace spanned by the basis vectors is not constrained, since the coefficients  $\alpha_j$  (or  $\alpha'_j$ ) can take on any values. Potentially, non-target spectra might be closely fit with the target basis set using unphysical coefficient values, resulting in false detections. In this paper we investigate two different constrained fitting methods that address this problem. In the first method, called "constrained SVD," SVD basis vectors are used with bounds on the fitting coefficients. In the second method, the basis vectors are target spectral endmembers, which define a simplex that follows the boundary of the subspace. Using positivity and sum-to-unity constraints, the pixel spectral fits lie inside the target simplex. We have implemented this approach with a sequential projection method used in the SMACC endmember algorithm [8,9], which is around an order of magnitude faster than standard constrained least-squares methods.

This paper presents results from these subspace methods with an LWIR image from the SEBASS hyperspectral sensor [10]. Two test cases are considered: known atmospheric parameters with unknown target range and surface temperature, and three unknown atmospheric parameters with unknown surface temperature. A preliminary account of this work has been reported [11]. We also describe the use of an atmospheric retrieval method to lower the subspace dimensionality, which results in significantly improved detection.

## 2. METHODOLOGY

### 2.1. Target Subspace Construction

The spectra defining the target subspace are constructed from a standard LWIR/MWIR radiation transport (RT) equation that relates a ground object's surface temperature  $T$  and emissivity spectrum  $e$  to the radiance  $L$  measured by a distant sensor [11]:

$$L = e t B(T) + (1-e)D(t) + P \quad (2)$$

The Eq. (2) parameters are implicitly wavelength-dependent. Transmittance  $t$ , path radiance  $P$  and downwelling illumination  $D(t)$  depend on atmospheric conditions. We have found that three dimensions of variability (air temperature, column water vapor and ozone concentration) are adequate for modeling the variations in  $t$ ,  $P$ , and  $D(t)$  over a wide range of conditions. The unknown  $T$  adds a fourth dimension to the target subspace. The target emissivity may be available from an independent measurement or derived from HSI data using atmospheric retrieval (AR) and temperature-emissivity separation (TES) procedures. We use an AR-TES code that is based on the work of Borel [2]. This code uses MODTRAN4<sup>TM</sup> [12] to construct a 3-D look-up table of  $t$ ,  $P$  and  $D(t)$  for a wide range of conditions, and retrieves emissivity and surface temperature on a pixel-by-pixel basis along with a single set of  $t$ ,  $P$  and  $D(t)$  spectra for the scene.

### 2.2. SVD Basis Sets and Fitting Procedures

SVD basis sets for non-mean-subtracted data are obtained as eigenvectors of the target subspace correlation matrix. Somewhat more efficient basis sets, representing mean-subtracted data, are similarly derived using the target subspace covariance matrix. The fitting coefficients in Eqs. (1a) and (1b) are the projections of the spectra onto the basis vectors. In our constrained method, the target subspace spectra are projected onto the basis vectors, the extrema of the coefficients for each basis function  $j$ , denoted  $\alpha_{jmin}$  and  $\alpha_{jmax}$ , are collected, and these extrema are used to bound the fits of the pixel spectra. That is, pixel spectrum projections less than  $\alpha_{jmin}$  or greater than  $\alpha_{jmax}$  are reset to  $\alpha_{jmin}$  or  $\alpha_{jmax}$ , respectively, in calculating the error residual.

### 2.3. Endmember Basis Set and Fitting Procedure

Endmember basis vectors for the target subspace were derived from the SMACC algorithm [9]. SMACC performs sequential projections to obtain both endmembers and their weighting factors in the spectral data. A variation on this procedure [8] enables constrained fitting of the image pixels using the target endmembers. The weighting factors resulting from these fits are the coefficients  $\alpha'_j$ , and the fitting error is calculated from Eq. (1b). The method yields a least-squares solution when the positivity constraint is inactive.

## 3. APPLICATIONS AND RESULTS

We have investigated a hyperspectral image from the airborne SEBASS sensor [10] taken at the Department of Energy's Atmospheric Radiation Monitoring site in Lamont, Oklahoma on June, 1997 at 21:21 LT from 1.5 km altitude. The data are described elsewhere [4]. The analyzed spectral channels are between 8 and 13  $\mu\text{m}$ , where the atmosphere has good transmission. The site has various ground covers (grass, water,

soil, and gravel), buildings, and calibrated emissivity panels. We analyzed two panel targets, a ~20-30% reflective panel and a near-blackbody panel. Ground truth reflectance measurements exist for the reflective panel.

Our AR-TES retrieved emissivity spectra agree quite well with ground truth measurements for various surfaces in the image. In the initial two test cases, retrieved emissivities define the target subspaces for the detection algorithm. Here the target pixel and its subspace representation agree to within the accuracy of the basis set fit, corresponding to the hypothetical case of perfect knowledge of the atmosphere. In Section 3.3 the use of ground truth reflectance is considered.

### 3.1. Case 1: Known Atmospheric Parameters, Unknown Target Range

We assume that the atmospheric profiles, and hence the  $t$ ,  $P$  and  $D(t)$  spectra, are reasonably well known, but that the target is at an uncertain distance from the sensor and has an unknown surface temperature. The atmospheric  $t$ ,  $P$  and  $D(t)$  spectra were taken from the AR-TES retrievals. Eq. (2) was then used to construct a target subspace comprised of 30 radiance spectra covering five different surface temperatures (295 to 310 deg K) and six different distances. Receiver-operator characteristic (ROC) curves that describe the detection of the panel pixels were constructed by calculating and thresholding the error residual from Eq. (1a) or (1b). Additional test cases were generated with Gaussian white noise added to the data.

Since the objective is to detect targets under a wide range of conditions, the algorithm was run on both the image and the 30-member target subspace, and the total number of correct detections recorded. The Figure 1 results, which include 5  $\mu\text{flicks}$  of added noise, show how detection varies with the SVD basis set. The curves are labeled with the number of basis vectors. The detection metric is the Eq. (1b) error with mean-subtracted data and the Eq. (1a) error with non-mean-subtracted data. However, using the Eq. (1b) error with the latter has little overall effect on the results. With three basis vectors there is a slight improvement upon constraining the coefficients (compare the solid and dotted lines). With fewer basis vectors the constraint has no effect. Best overall performance is found with two basis vectors, equaling the number of subspace dimensions.

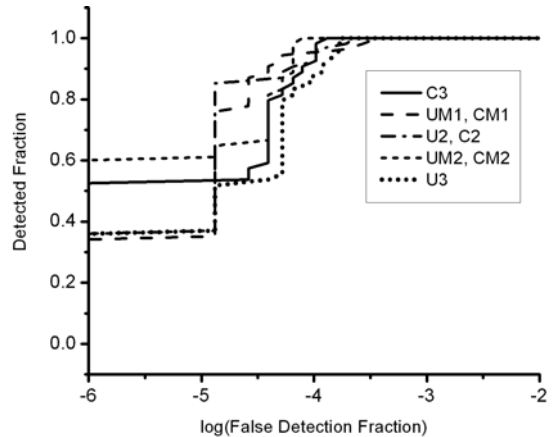


**Figure 1.** ROC curves for reflective panel detection at unknown range using SVD basis sets. Key: U = unconstrained, C = constrained, M = target mean-subtracted data.

Results using endmember basis sets were reported previously [11]. They are much less sensitive to the number of basis vectors than the SVD results; four-endmember and seven-endmember ROC curves overlap over most of their range. Performance is comparable to the best SVD basis sets.

For the harder-to-detect near-blackbody panel, 2  $\mu$ flicks of noise was added to the data. As with the reflective panel, the constraints have no effect when the optimum number of basis vectors is used. However, here three basis vectors are better than two. The results from six- and eight-endmember basis sets, which fit the panel subspace to within respectively 1 and 0.5  $\mu$ flick, are comparable to the three-vector SVD results [11].

### 3.2. Case 2: Unknown Atmospheric Parameters

For this case, the target subspace was based on a 60-element, 3-D look-up table of atmospheric  $t$ ,  $P$  and  $D(t)$  spectra generated by our AR-TES code. These cover a 40 deg C range in surface air temperature, a factor-of-four range in column water vapor, and factor-of-two range in column ozone. Each  $t$ ,  $P$ ,  $D(t)$  combination was used in Eq. (2) together with the target emissivity and five surface temperatures, yielding a 4-D target subspace of 300 spectra. As in Case 1, 5  $\mu$ flicks RMS of Gaussian noise was added to the data.

Results for detection of the reflective panel are shown in Figure 2. Here only the targets in the image are being searched for. The SVD results use mean subtraction and the Eq. (1b) error metric. Very similar results, not shown, were obtained using non-mean-subtracted data with either Eq. (1a) or (1b).

The endmember method results display little if any variation with the basis set size between 14 and 29 endmembers; only the former is shown. Their performance is much worse than that of the SVD basis sets, most likely because the target fitting error remains much larger than the noise level. These poor fits may reflect a deficiency in the SMACC endmember selections. Much better fits are however obtained with the near-blackbody target, where there is little difference in performance between the endmember and SVD basis sets. Similar to Case 1, constraints provide little overall difference in performance with SVD basis vectors when the basis set is small. However, they provide a modest improvement with six basis vectors.

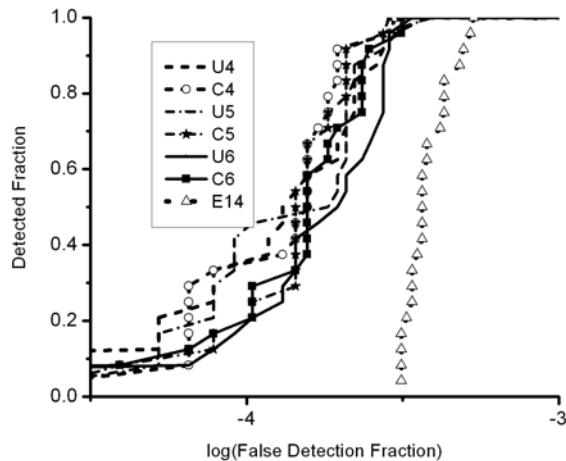


Figure 2. ROC curves for reflective panel detection under unknown atmospheric conditions.

### 3.3. Unknown Versus Known or Retrieved Atmospheric Parameters

For an initial study of the use of known or retrieved atmospheric parameters to reduce the target subspace dimensionality, the 2-D Case 1, making use of known parameters, was rerun for the image-only targets and compared with the 4-D Case 2. Results are shown in Figure 3 for the top-performing basis sets. With known atmospheric parameters there is a dramatic improvement in detection (compare the Retrieved C2 and C4 curves). Here the false detections are mainly from an adjacent, similarly reflective panel and from pixels that are partially filled with reflective building roofs.

For a more realistic test, mimicking the operation of a sensor system, the target subspaces were constructed from the ground truth reflectance spectrum rather than from the AR-TES retrieval. The results are shown as the Truth curves in Figure 3. Here performance is compromised by inaccuracies in both the AR-TES atmospheric retrieval and the target subspace representation. These may include SEBASS sensor calibration inaccuracy as well as limitations in the accuracy and completeness of the MODTRAN™ calculations in the AR-TES code. While detection is uniformly poorer than with the retrieved emissivity, the 2-D subspace, which here makes use of less-than-perfect atmospheric information, is again superior to the 4-D subspace. Interestingly, in the 4-D case the endmember basis set performs better overall than the SVD basis set.

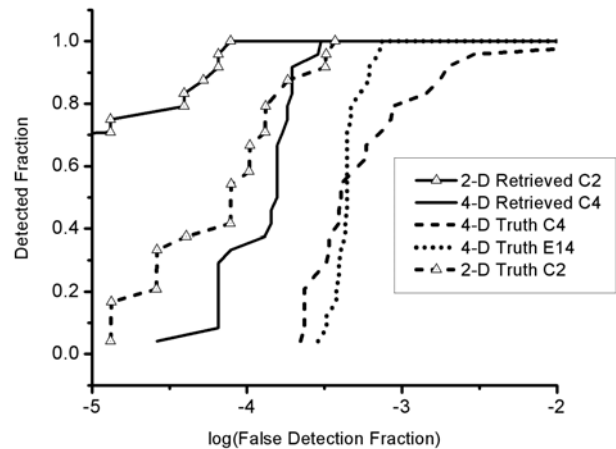


Figure 3. ROC curves for reflective panel detection under retrieved (2-D subspaces) and unknown (4-D subspaces) atmospheric conditions. Subspaces were constructed from retrieved or ground truth emissivity spectra, as indicated.

## 4. SUMMARY AND CONCLUSIONS

This paper describes the application of constrained basis sets for target subspaces to HSI whole-pixel detection problems. The detection metric is based on the accuracy of the basis set fits to the pixel spectra. One method uses SVD basis vectors with the fitting coefficients bounded by the target subspace. Another uses endmember basis vectors with sum-to-unity and positivity constraints on the fits. Two thermal IR test cases were considered: (1) known atmospheric parameters but unknown target range and surface temperature, and (2) three unknown atmospheric

parameters and unknown surface temperature. The constrained methods improve detection robustness by reducing over-fitting when too many basis vectors are used. With inclusion of a background subspace, constrained methods may prove similarly helpful for sub-pixel detection.

We have also begun investigating the relative merits of subspace simulation-based and atmospheric retrieval approaches in the thermal IR. An advantage of the latter is that an atmospheric homogeneity assumption constrains the atmospheric parameters to be consistent across all pixels. Initial results suggest that atmospheric retrievals performed with current thermal IR hyperspectral datasets and algorithms are accurate enough to allow reduction of the target subspace by several dimensions, leading to improved detection. Healey and Ratkowski [13] also note the inverse relationship between detection performance and subspace size, although their subspace reduction was achieved using weather data rather than the imagery itself. With less accurate atmospheric information, dimensionality reduction may prove problematic, whereas constrained basis sets might be used to bound the atmosphere within an estimated retrieval uncertainty.

## 5. ACKNOWLEDGEMENTS

The authors are grateful to Dr. J. Romano (US Army ARDEC, Picatinny Arsenal) for program guidance and Drs. Marsha Fox and Lawrence Bernstein (Spectral Sciences, Inc.) and Alan Stocker (Space Computer Corp.) for helpful technical discussions. This work was funded by the US Army under Contract No. W15QKN-07-C-0008.

## 6. REFERENCES

1. M.W. Matthew, S.M. Adler-Golden, A. Berk, G. Felde, G.P. Anderson, D. Gorodetzky, S. Paswaters and M. Shippert, "Atmospheric Correction of Spectral Imagery: Evaluation of the FLAASH Algorithm with AVIRIS Data," *SPIE Proc, Algorithms and Technologies for Multispectral, Hyperspectral, and Ultraspectral Imagery IX* (2003).
2. C.C. Borel, "ARTEMISS – an Algorithm to Retrieve Temperature and Emissivity from Hyper-Spectral Thermal Image Data," *28th Annual GOMACTech Conference, Hyperspectral Imaging Session*, Tampa, FL, Los Alamos National Lab. Rpt. No. LA-UR-027907 (2003).
3. E.D. Hernandez-Baquero and J. R. Schott, "Atmospheric compensation for surface temperature and emissivity separation," *SPIE Proceedings, Algorithms for Multispectral, Hyperspectral, and Ultraspectral Imagery VI*, Vol. 4049, pp. 400-410 (2000).
4. S.J. Young, B.R. Johnson and J.A. Hackwell, "An In-scene Method for Atmospheric Compensation of Thermal Hyperspectral Data," *J. Geophys. Res. Atmospheres*, Vol. 204, pp. ACH 14-1 – ACH 14-20 (2002).
5. G. Healey and D. Slater, "Models and Methods for Automated Material Identification in Hyperspectral Imagery Acquired Under Unknown Illumination and Atmospheric Conditions," *IEEE Trans. Geosci. Remote Sensing*, 37, 2706-2717 (1999).
6. B. Thai and G. Healey, "Invariant Subpixel Material Detection in Hyperspectral Imagery," *IEEE Trans. Geosci. Remote Sensing*, 40, 599-608 (2002).
7. P. Bajorski, E.J. Ientilucci and J.R. Schott, "Comparison of Basis-Vector Selection Methods for Target and Background Subspaces as Applied to Subpixel Target Detection," *Algorithms and Technologies for Multispectral, Hyperspectral, and Ultraspectral Imagery X*, Sylvia Shen and Paul Lewis, eds., *Proc. SPIE* 5425, 97-108 (2004).
8. J. Gruninger and S. Adler-Golden, "Process for Finding Endmembers in an Image," U.S. Patent Pending (2006).
9. J.H. Gruninger, A.J. Ratkowski, and M.L. Hoke, "The Sequential Maximum Angle Convex Code (SMACC) Endmember Model," *Algorithms and Technologies for Multispectral, Hyperspectral, and Ultraspectral Imagery X*, Sylvia Shen and Paul Lewis, eds., *Proc. SPIE* 5425, 1-14 (2004).
10. J.A. Hackwell, D.W. Warren, R.P. Bongiovi, S.J. Hansel, T.L. Hayhurst, M.G. Sivjee, and J.W. Skinner, "LWIR/MWIR imaging hyperspectral sensor for airborne and ground-based remote sensing," *SPIE Proceedings, Imaging Spectrometry*, Vol. 2819, pp. 102-107 (1996).
11. S. Adler-Golden, J. Gruninger and R. Sundberg, "Constrained basis set expansions for target subspaces in hyperspectral detection and identification," *Algorithms and Technologies for Multispectral, Hyperspectral, and Ultraspectral Imagery XIV, SPIE Defense and Security*, Orlando, FL, March 2008, in press.
12. A. Berk, L.S. Bernstein, G.P. Anderson, P.K. Acharya, D.C. Robertson, J.H. Chetwynd and S.M. Adler-Golden, "MODTRAN Cloud and Multiple Scattering Upgrades with Application to AVIRIS," *Remote Sens. Environ.* 65:367-375 (1998).
13. G. Healey and A. Ratkowski, "Atmospheric sampling for hyperspectral signature modeling," *Algorithms and Technologies for Multispectral, Hyperspectral, and Ultraspectral Imagery XIV, SPIE Defense and Security*, Orlando, FL, March 2008, in press.